A facile route for the synthesis of reduced graphene oxide (RGO) by DVD laser scribing and its applications in the environment-friendly electrochromic devices (ECD)

A. BUASRI[a,b*], T. ANANGANJANAKIT[a], N. PEANGKOM[a], P. KHANTASEMA[a], K. PLEERAM[a], A. LAKAEO[a], J. ARTHNUKARN[a], V. LORYUENYONG[a,b*]

[a]*Department of Materials Science and Engineering, Faculty of Engineering and Industrial Technology, Silpakorn University, Nakhon Pathom 73000, Thailand*

[b]*Center of Excellence on Petrochemical and Materials Technology, Chulalongkorn University, Bangkok 10330, Thailand*

Electrochromism refers to the reversible change of color of thin films due to a small change in the voltage. This mechanism is important for smart windows and display applications. In this work, the use of laser-scribed graphene oxide (LSGO) and biodegradable polymers as the environment-friendly electrochromic devices (ECD) was reported. Reduced graphene oxide (RGO) or LSGO was prepared by using modified Hummer's method and laser scribing DVD burner. Poly(lactic acid) (PLA) and poly(butylene succinate) (PBS) films were coated with LSGO by drop-casting method. The materials were analyzed by X-ray diffraction (XRD), Fourier transform infrared (FT-IR) spectroscopy, Raman spectroscopy, scanning electron microscopy (SEM), transmission electron microscopy (TEM), energy dispersive spectroscopy (EDS), electrical resistance measurements and cyclic voltammetry (CV). The carbon (C) content reached to a maximum (90.15 at%) and the oxygen (O) content reached a minimum (6.51 at%) when the laser irradiation was 10 times. The poly(2,2-dimethyl-3,4-propylenedioxythiophene) (PProDOT-Me_2) and polyaniline (PANI) also were electroactives and had good adhesion towards LSGO substrate. Our results primarily indicated that the PLA/LSGO/PProDOT-Me_2 device offered an optical modulation, in which the color of the device switched from dark blue to a fully transparent state under the applied potential at $\pm$ 1 V within 5 s. In addition, the thin film of PANI had good stability and reversibility. The PBS/LSGO/PANI device had four different colors (yellow, green, blue and violet). This novel configuration presented an easy, expeditious and green way of preparing ECD. It was fabricated using a single-layer polymer. The LSGO in the flexible ECD demonstrated a potential for replacing indium tin oxide (ITO) in flexible electrochromic windows.

(Received August 19, 2016; accepted August 9, 2017)

Keywords: Laser-scribed graphene oxide, Reduced graphene oxide, Biodegradable polymer, Environment-friendly device, Electrochromic, Transparent conductive electrode

1. Introduction

Electrochromism (EC), a reversible change of color in a material's optical properties under an applied voltage, is an old phenomenon, which was discovered 40 years ago [1]. The color change takes place because of intercalation and deintercalation of ions, which is controlled by voltage applied between transparent conductive oxide (TCO) layers. The simplest solid electrochromic device (ECD) consists of three layers: TCO, EC active layer and electrolyte [2]. The applications of EC materials have been extended to smart windows, displays, antiglare mirrors and active camouflages [3]. EC smart windows are the devices that can change from transparent to frosted and to opaque with the simple turn of a switch. They are really the best candidate for energy-efficient applications and a promising solution for controlling the amount of heat or light entering a building, and reducing heating, air-conditioning and lighting costs [4].

Graphene, a two dimensional sheet of sp^2-hybridized carbon system, has been an attractive material in the past few years due to its unique electrical, optical, thermal and mechanical properties. It is, therefore a suitable candidate for many applications such as nanoelectronics, nanocomposites, nanomedicine, chemical and biological sensors, supercapacitors [5-8]. Graphene nanosheets have been prepared by several approaches such as micromechanical cleavage, epitaxial, reduction of graphite oxide (GPO) and graphene oxide (GO) [9]. Among them, the reduction of GO has emerged as an attractive approaches. Different reduction processes can be performed, including chemical reduction via hydrazine derivatives or other reducing agents, high-temperature annealing under chemical reducing gases and/or inert atmospheres, solvothermal reduction, a combination of chemical and thermal reduction methods, flash reduction, and most recently, laser reduction of GO [10].

Interestingly, the fabrication of reduced graphene oxide (RGO) films as stand-alone electrodes has been demonstrated as a route to fabricate supercapacitors and ECD. The cost-effective process involves the simplification of the laser source and the generation of laser-scribed graphene (LSG) or laser-scribed graphene oxide (LSGO) as a new member of the graphene family.

With this method, LSG or LSGO is produced by thermally reducing a film of GO at predefined positions using a LightScribe DVD burner. The laser-scribed areas could be very effectively reduced by a rapid expansion and exfoliation of the layers, producing a film with excellent conductivity, high porosity, flexibility, and a specific surface area as high as 1,520 m^2/g^{-1} [11]. El-Kady et al. have been successfully fabricated graphene over large area by a standard laser scribing DVD burner [12]. The LSG films possess open pores which facilitate the electrolyte accessibility to the surfaces of films [13]. Laser scribing technique is, therefore, an attractive graphene growth and patterning technology, owing to its low cost, time saving, and flexibility.

Indium tin oxide (ITO) has been used commonly as a transparent conductive electrode (TCE) due to its low resistivity and high transmittance. However, ITO is chemically instable and mechanically brittle. It has a demerit for application in flexible devices (low conductivity upon bending). For these reasons, graphene and its derivatives have been studied as an alternative TCE for the replacement of ITO [14]. The replacement of traditional glass substrates by polymeric materials has attracted considerable interest in the field of flexible electrochromic applications. Several types of biopolymers have been explored to develop the environment-friendly ECD. Poly(lactic acid) (PLA) and poly(butylene succinate) (PBS), the increasingly popular polymer, have spurred extensive attention in the recent decades for the academic and industrial research due to their effective biodegradability in industrial compost environments and availability from renewable resources such as starch and sugar [15-17]. Herein, PLA and PBS have been, therefore, selected as the biopolymer substrates in this study.

There are lots of studies focused on using graphene and its derivatives to improve the performance of ECD. Literature reviews showed that the LSGO-coated PLA or PBS electrodes have never been used as the working electrode for flexible devices in electrochromic applications. In our work, the synthesis of GO from chemical oxidation of graphite, followed by the reduction of the produced GO into LSGO via laser scribing DVD burner was focused. The LSGO was then coated on the biopolymer supports for the use as TCE. The fabrication and evaluation of a prototype of the environment-friendly ECD based on a single-layer polymer such as poly(2,2-dimethyl-3,4-propylenedioxythiophene) (PProDOT-Me_2) or polyaniline (PANI) structure with the following configuration: i.e. PLA/LSGO/PProDOT-Me_2/LSGO/PLA and PBS/LSGO/PANI/LSGO/PBS was also described.

2. Experimental details

2.1. Materials

Graphite fine powder extra pure (purity 98%) and hydrochloric acid (HCl) 37% were purchased from Merck Ltd., Germany. Sulfuric acid (H_2SO_4) 98% Grade AR was purchased from RCI Labscan Ltd., Thailand. Potassium permanganate ($KMnO_4$) and sodium nitrate ($NaNO_3$) were purchased from Ajax Finechem PTY Ltd., Australia. Hydrogen peroxide (H_2O_2) 30-32% Grade AR was purchased from QReC Chemical Co. Ltd., Thailand. 2,2-dimethyl-3,4-propylenedioxythiophene (ProDOT-Me_2) was synthesized according to the reported procedure [18]. Aniline monomer (ANI) 99% was purchased from Panreac AppliChem, USA. PLA film (Grade 4043D, cast sheet co-extrusion, National Metal and Materials Technology Center (MTEC), Thailand) and PBS film (grade 5B0900919H, Thai KK Industry Co., Ltd., Thailand) were used as biopolymer substrates of ECD. All chemicals used were analytical grade reagents.

2.2. Preparation of GPO, GO and LSGO

GPO was prepared by modified Hummer's method using graphite fine powder as a starting material [19]. The synthesis procedure is described as follows: 5.0 g graphite, 2.50 g $NaNO_3$ and 90 mL concentrated H_2SO_4 were added into a 500 mL flask kept at 5 °C in a bath ice under continuous stirring for 2 h. Then, 15.0 g $KMnO_4$ was slowly added into the flask to prevent strong reaction at local points. The reaction mixture was maintained at 5 °C for 2 h, and then the reaction temperature was slowly raised to 35 °C and kept for another 30 min with vigorous stirring. 240 mL Distilled water was added into the suspension and, as a consequence of the hydration, the temperature was raised to 80 °C. The bath was kept at this temperature for 2 h with stirring. H_2O_2 (30% v/v, 10 mL) was then added to the mixture to stop the reaction and to reduce the residual $KMnO_4$. The resulting product had a brown/yellowish color and was separated from the solution by vacuum filtration. The solid was washed with diluted HCl aqueous solution (5%, 800 mL) to remove the remnant Mn ions and with distilled water to remove the acid until the pH were 6. The GPO was dried at 60 °C for 24 h.

Aqueous colloids of GO were prepared by dispersing 5.0 g GPO into 250 mL of distilled water by ultrasonication and centrifugation for 2 h to remove any unexfoliated GPO. The obtained GO had a golden-brown color and was dried at 60 °C for 2 h [20].

GO dispersion in water with 0.06 g/mL concentration was then prepared for the production of GO films on the substrate. About 5 mL of the solution was then drop-casted on a DVD media disc, and then dried at 40 °C for 2 h. After that, the disc was inserted into a LightScribe DVD drive (LG GP40LB10). The laser inside the drive (λ = 780 nm, Power 38 = mW) then converted the GO into black LSGO layer in one-stop process. The laser scribing technology makes it possible to obtain the large-area of precise patterns of graphene and its derivatives in 20 minutes for each cycle [21]. In addition, the number of cycles used for the laser reduction of a film results in a significant and controllable change in sheet resistance [10]. In this experiments, the laser irradiation was repeated 10 times (10 cycles of LightScribe) to ensure the maximized reduction process.

Fig. 1 showed the preparation process of GPO, GO and LSGO from graphite by using modified Hummer's method and laser scribing DVD burner. During the oxidation process, graphite powder was treated with strong oxidizing agents and introduced oxygen-containing functional groups into GPO. After ultrasonication and laser reduction, the oxygen-containing functional groups were removed, and the LSGO sheet was obtained [22].

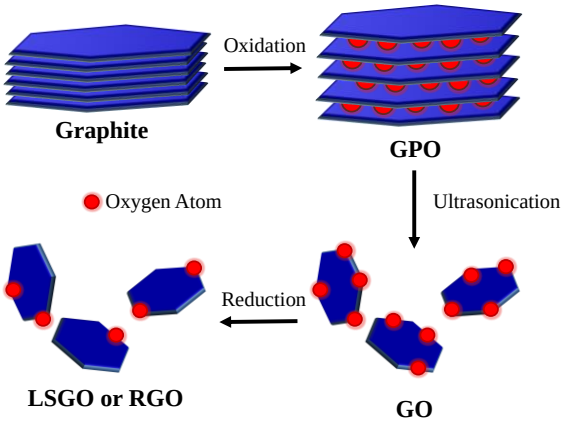

Fig. 1. Preparation of GPO, GO and LSGO by chemical oxidation and laser reduction.

A schematic of the reduction process (laser scribing method) can be seen in Fig. 2. This one-step patterning process can be carried out in any lab with basic computer facilities and requires no masks, or expensive lithography, for the microfabrication of electrochemical sensors [11]. LightScribe technology was invented by Hewlett-Packard (HP) for direct disc labeling process. In this process, the surface color of the disc will change to a darker shade when exposed to light. The wavelength of the optical system uses 780 nm which will create etches on the surface of the LightScribe disc. A LightScribe enabled DVD drive uses an optical laser to burn an image into the thin dye coating on the label side of a LightScribe disc [23].

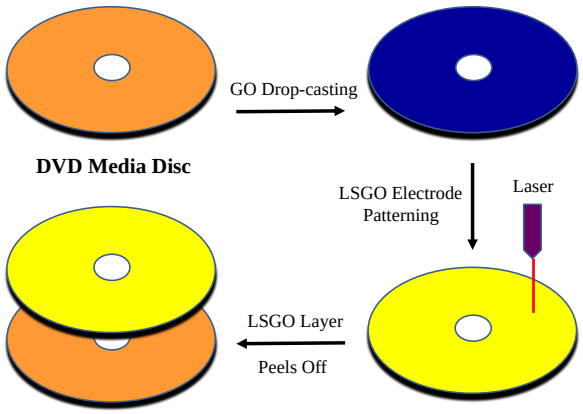

Fig. 2. The process of patterning LSGO electrodes on a DVD media disc

2.3. Electrochromic device assembly

0.15 g LSGO layer was first dispersed in 1 mL water by ultrasonication for 10 min. A drop of LSGO suspension was placed on a 2.5 cm x 2.5 cm PLA or PBS substrate (300 μm in thickness) using a scotch tape mask and a sharpened blade via doctor-blade technique. The film thickness was controlled by scotch tape. The resulting graphene derivative-based coating layer had a very uniform thickness (~10 μm). The PLA or PBS film coated with LSGO was then dried at 40 °C for 6 h.

Fig. 3 represents schematic presentation of the environment-friendly ECD. This device consists of three layers: biopolymer substrate, LSGO-based TCE, electrolyte and EC active layer. With LSGO coated biopolymer, the devices would have higher flexibility and biodegradeability than ITO coated glass slide. It has then been studied as the TCE in ECD for the replacement of ITO in this study.

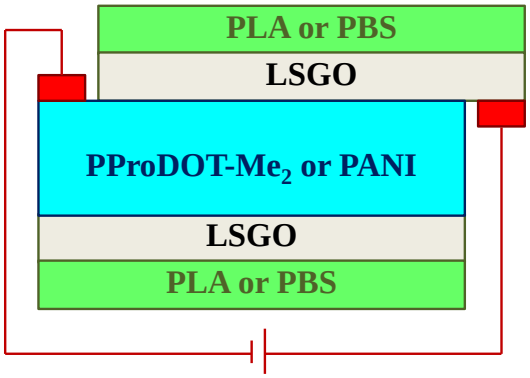

Fig. 3. Schematic diagram of ECD consisting of a single-layer polymer

The preparation of liquid monomer and polymer electrolytes were prepared according to the work reported by Zhu et al. [24] and Zainal et al. [25]. Based on those works, the monomer (ProDOT-Me_2) could be converted into electrochromic polymer (PProDOT-Me_2) under a constant potential of +3 V for an appropriate conversion time. Fig. 4 shows a schematic diagram for the in situ polymerization of monomer electrolyte and electrochromic monomer.

The electrochemical deposition of PANI was carried out using three electrode systems (Autolab, Potentiostat/Galvanostat Instrument) with LSGO-coated PBS as a working electrode, platinum rod as a counter electrode and Ag/AgCl as a reference electrode. All ECD were cycled between their bleached and colored states at ± 1.2 V five times before data was recorded.

2.4. Materials characterization

Crystallographic information on the samples was obtained using a powder X-ray diffractometer (XRD, LabX XRD-6100, Shimadzu, Japan) with Ge(1 1 1) monochromatized CuKα radiation (λ = 1.542 Å) having a scanning speed of 2°/min. Diffraction data were collected

over the 2θ range from 5 to 40°. The presence of various functional groups in the GPO, GO and LSGO were measured using Fourier transform infrared (FT-IR) spectrometer (Model: Bruker Optics, Vertex70, Germany). Raman spectra of the materials were measured using a Fourier transform Raman (FT-Raman) spectrometer (Model: Perkin Elmer, Spectrum GX, USA) with Ar^+ laser (532 nm) over the 500-3000 cm^{-1} range. The morphologies of the resulting products were characterized using the scanning electron microscope (SEM, Hitachi TM3030, USA) and transmission electron microscope (TEM, JEOL JEM-1230, USA). The energy dispersive spectroscopy (EDS) was used to determine the elemental composition of manually chosen areas in the GO and LSGO. The electrical characterization of LSGO coated on PLA or PBS film was measured by four-point probe technique (S-302-4, Lucas Labs, Canada). Five measurements were performed on different areas of each sample to ensure reproducibility. Finally, all electrochemistry was performed using a PGSTAT 101 Potentiostat/Galvanostat (Metrohm Autolab B.V., Netherlands) for cyclic voltammetry (CV) analysis. A UV-A (365 nm, 20 W) lamp unit (FIRST and FERN Co., Thailand) was used to cure the liquid monomer electrolyte (ProDOT-Me_2).

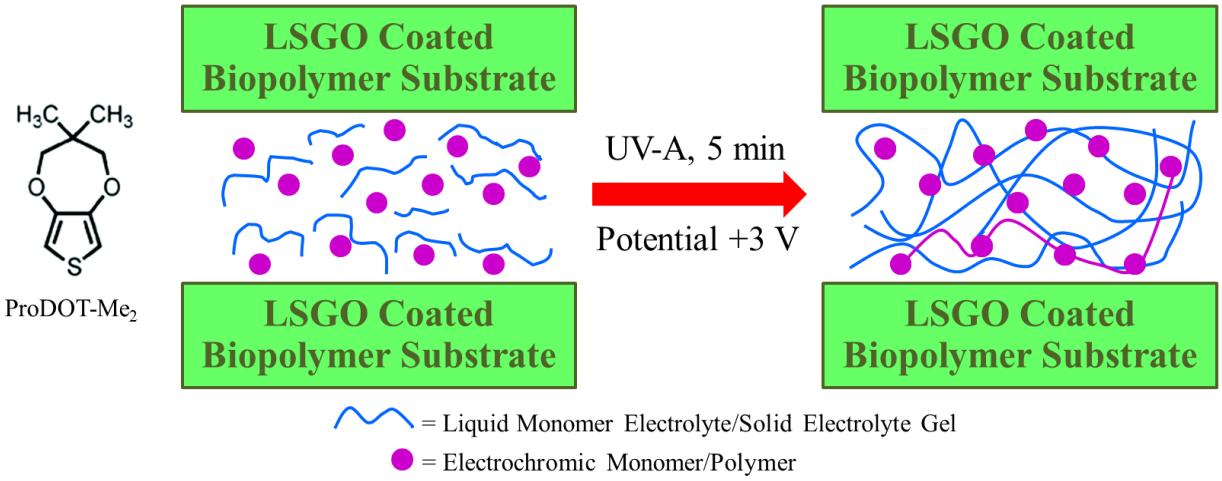

Fig. 4. Schematic diagram for in situ polymerization of liquid monomer electrolyte and electrochromic monomer

3. Results and discussion

3.1. Characterization of graphite, GPO, GO and LSGO

XRD is a useful tool to assess the efficiency of the process by monitoring the crystal structure. Fig. 5 shows XRD patterns of graphite, GPO, GO and LSGO. Raw graphite showed a very strong and sharp (0 0 2) peak at 2θ = 26.38° (d-spacing = 0.34 nm). In comparison, a (0 0 1) peak at 2θ = 11.12° (d-spacing = 0.79 nm) is observed for GPO, which clearly indicates the damage of the regular crystalline pattern of graphite during the oxidation, in consistent with previous literatures [26]. The interlayer distance of GO is approximately 0.81 nm which is larger than that of graphite and GPO. This phenomenon can be attributed to the introduction of oxygen-containing functional groups into the carbon lattice during the expanding process. The values of d-spacing indicates that the laminar distance of graphite layers have been efficiently increased in the vertical direction throughout the chemical oxidation and exfoliation process [27]. After laser reduction, the (0 0 1) peak at 2θ = 10.94° of GO disappeared and a broad peak appeared at 2θ = 24.10°. This result illustrates a decrease in interlayer distance of LSGO (d-spacing = 0.37 nm) and the removal of oxygen functional groups [28].

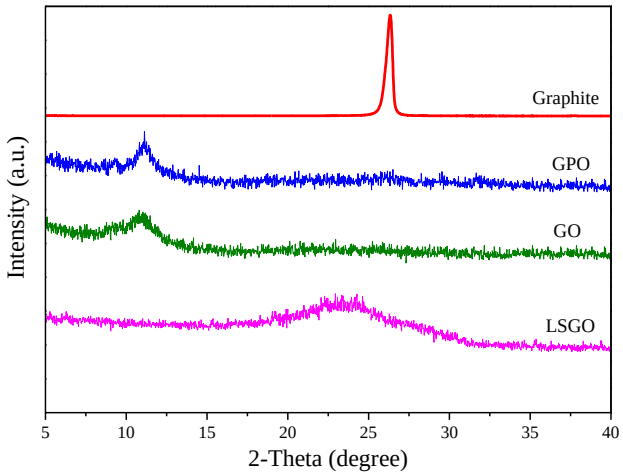

Fig. 5. XRD patterns of graphite, GPO, GO and LSGO

Fig. 6 shows the FT-IR spectra of graphite, GPO, GO and LSGO. The characteristic bands of graphite at 3450, 1641 and 1593 cm^{-1} are assigned to –OH, C=C stretching of the benzenoid rings and –Ph, respectively [26]. The spectrum of GPO illustrates the presence of C–O (ν_{C-O} at 1060 cm^{-1}), C–O–C (ν_{C-O-C} at 1255 cm^{-1}), C–OH (ν_{C-OH} at 1370 cm^{-1}), and C=O in carboxylic acid and carbonyl moieties ($\nu_{C=O}$ at 1720 cm^{-1}). The peak at 1600 cm^{-1} may be resulted from skeletal vibrations of unoxidized

graphitic domains [29]. The characteristic features of GO are the bands at 1055 cm^{-1} (C–O stretching vibrations), 1380 cm^{-1} (C–OH stretching vibrations) and 1720 cm^{-1} (C=O stretching vibrations from carbonyl and carboxylic groups). The peak at 1650 cm^{-1} is most possibly due to the skeletal vibration of graphitic domains. Apart from these sharp features, the broad peak around 3000–3650 cm^{-1} is assigned to hydroxyl groups, and the peak at 2920 cm^{-1} is from $–CH_2$ stretching [30]. The spectrum of LSGO shows a peak at 3400 cm^{-1}, representing O–H stretching vibrations, which was significantly reduced due to deoxygenation. The C=O at 1730 cm^{-1} in this spectrum is due to the expansion of carbon dioxide (CO_2) evolved into the interstices between the RGO sheets during rapid laser scribing. The C–O stretching vibrations observed at 1050 cm^{-1} are due to the remaining carbonyl groups after the reduction process by a LightScribe DVD drive [6].

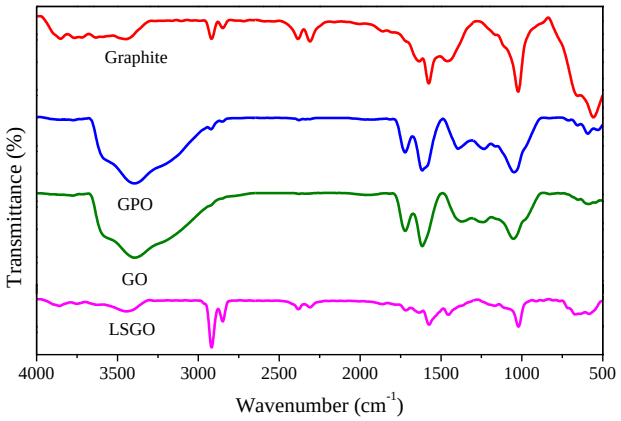

Fig. 6. FT-IR spectra of graphite, GPO, GO and LSGO

The significant structural changes occurring during the chemical and physical processing from graphite powder to LSGO are reflected in their Raman spectra (Fig. 7). The Raman spectrum of graphite displays a prominent G-band at 1582 cm^{-1}, corresponding to the first-order scattering of the E_{2g} mode observed for the sp^2-domains [31] and a 2D band with a peak profile at 2730 cm^{-1}. It also shows D-band at 1352 cm^{-1} which is assigned to edge planes, defects and disordered structures of carbons found in graphene sheets. The intensity of D-band is higher than that of G-band in both GPO and GO. In comparison to graphite powder, significant changes observed in both the G-band and the D-band implies some modification of graphite into amorphous carbon containing a certain fraction of sp^3-carbons. In addition, the G-band of GPO and GO broadens and shifts toward higher wavenumbers (1592 cm^{-1}). The intensity ratio of D/G-bands (I_D/I_G) for the graphite powder is 0.2 and 1.1 for the GPO and GO (Table 1). An increase in intensity ratio of material indicates the dramatic loss of order from graphite to GPO and GO [32]. After reduction of GO to LSGO by laser scribing DVD burner, the D band and G band shifted toward lower frequency region (1351 and 1583 cm^{-1}), confirming the reduction mechanism. The D/G-bands intensity ratio of LSGO sample (1.2) is larger than that of GO, which confirms that might be due to the removal of functional groups and formation of defects [33,34].

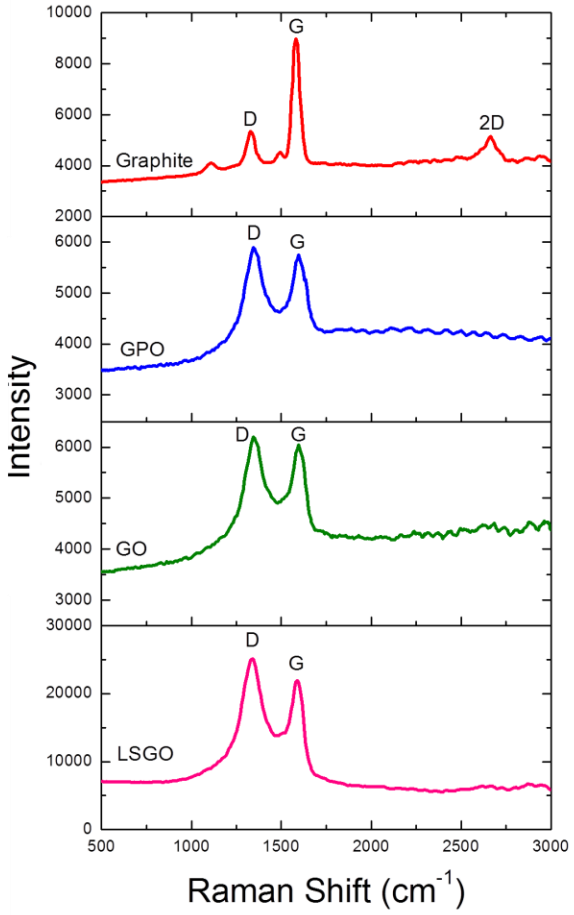

Fig. 7. Raman spectra of graphite, GPO, GO and LSGO

Morphological characterization of the graphene derivative nanosheets was conducted using SEM and TEM. As shown in Fig. 8, the SEM and TEM images of exfoliated samples exist as typical wrinkled structure, folded region, transparent, indicating that these layers are exfoliated to a very large extent [35]. The LSGO nanosheets are well organized and so thin that electron beam can be passed through sample. The transparency of the LSGO nanosheet suggests a thin thickness of the film. However, some areas of LSGO nanosheets are restacking and exhibit morphology similar to wrinkled paper. The superficial wrinkles are probably caused by aggregation of LSGO nanosheets during the preparation process [13]. As reported previously, corrugation and scrolling are intrinsic to graphene derivative nanosheets. This is because the thermodynamic stability of the 2D membrane results from microscopic crumpling via bending or buckling [27].

Energy dispersive spectra were obtained from the SEM images and acquired in different points of each samples. For the GO and LSGO prepared by the modified Hummer's method and laser scribing DVD burner, the EDS results were illustrated in Table 2. As shown, the modified Hummers' GO has a mean carbon (C) contents around 65 at% and an oxygen (O) contents around 30 at%,

giving C/O = 2.13 accounting for the 95.88% of the total atomic composition. The remaining 4.12 at% consists of potassium (K), sulfur (S), sodium (Na), calcium (Ca) and other impurities, possibly coming from the inadequate purification of raw materials and laboratory (each of them below 0.2 at%). In the LSGO sample, the C content has a steady increase, while the O content continues to decline as the number of laser irradiation cycles is increased. The C content reached to a maximum, and the O content reached to a minimum when the laser irradiation was 10 times (LSGO-10). Nevertheless, based on the elemental analysis (EA), 10 cycles of laser irradiation were selectively performed throughout the experiment. The results indicate that some residual functional groups still exist on the surface of LSGO, although most of them have been removed during the laser reduction [36].

Table 1. Raman results of graphite, GPO, GO and LSGO

Type of material	Graphite	GPO	GO	LSGO
Intensity Ratio of D/G-bands (I_D/I_G)	0.2	1.1	1.1	1.2
Position of D-band (W_D : cm^{-1})	1352	1359	1359	1351
Position of G-band (W_G : cm^{-1})	1582	1592	1592	1583

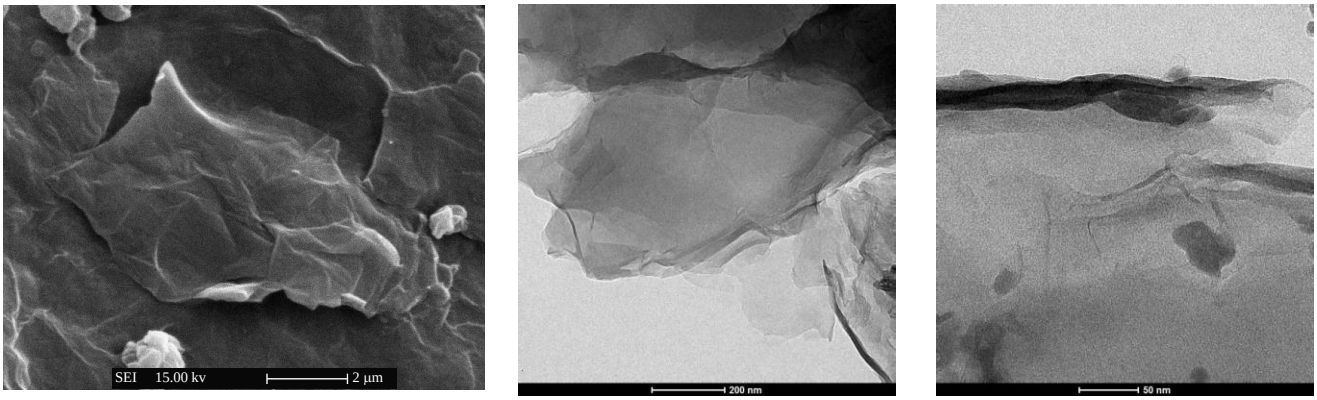

(a) (b) (c)

Fig. 8. SEM (a) and TEM (b), (c) images of LSGO

Table 2. EDS results of GO and LSGO from SEM images

Type of sample	Element content (at%)		
	Carbon (C)	Oxygen (O)	Other elements (such as K, S, Na and Ca)
GO	65.25	30.63	4.12
LSGO-1 (1 time)	82.21	14.21	3.58
LSGO-10 (10 times)	90.15	6.51	3.34

As a direct indication of reduction process, Table 3 shows the sheet resistance of GPO, GO and LSGO. The sheet resistances of both GPO and GO were very high. These materials are known to be the insulating materials due to the extensive presence of saturated sp^3 bonds, the high density of electronegative oxygen atoms bonded to carbon, and other defects that give rise to an energy gap in the electron density of states. RGO, on the other hands, recovers the conductivity by partial restoration of the sp^2 hybridization and C=C conjugation. The values of sheet resistance decreased after the laser reduction of GO and depend on the degree of reduction [36]. The resistance values of LSGO-1, LSGO-3, LSGO-5 and LSGO-10 are 133, 109, 88 and 17 Ω/sq, respectively. It can then be noted that LSGO can be reduced by the laser scribing technique. The electrical conductivity of all carbon materials depends on the density; denser materials have higher electrical conductivity [37]. In addition, the number of times a film is laser-treated results in a significant and controllable change in sheet resistance, a property that has so far been difficult to control through other methods [10].

Table 3. Sheet resistance data of GPO, GO and LSGO

Type of material	GPO	GO	LSGO-1	LSGO-3	LSGO-5	LSGO-10
Sheet Resistance (Ω/sq)	Not Detected (Insulator)	Not Detected (Insulator)	133	109	88	17

3.2 Application of LSGO and biopolymers in ECD

The electrochemical measurements such as electrochemical behavior and electrochemical stability were measured using CV technique. The electrodes coated with electropolymerized conducting polymer films have been paid great attention due to their unique physical and chemical properties and electrocatalysis [38].

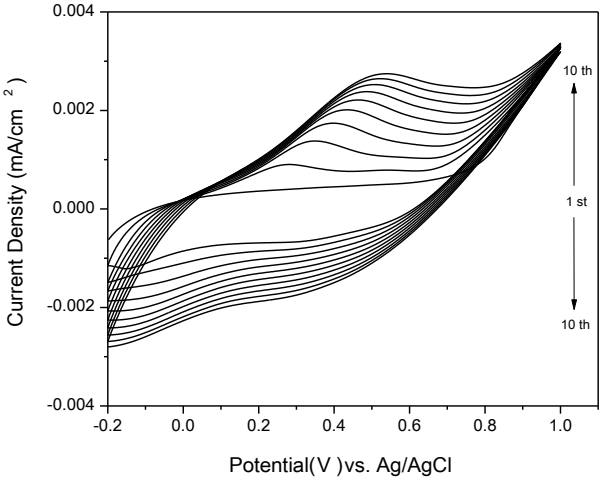

Fig. 9. Cyclic voltammograms of LSGO-coated PBS working electrode scanned for 10 cycles in the potential range from -0.2 V to + 1.0 V vs Ag/AgCl reference electrode at scan rate of 50 mV/s.

The cyclic voltammograms of LSGO-coated PBS working electrode in acidic solution of 1 M H_2SO_4 containing 0.5 M aniline monomer are represented in Fig. 9. The voltammograms were scanned from -0.2 V to +1.0 V. It was found that, for the first cycle, the current started to increase at +0.7 V, indicating the polymerization onset of aniline on the LSGO surface. This means that PANI starts to deposit on LSGO surface at +0.7 V. On the second cycle, the amount of PANI deposited on the LSGO surface increased as the current density increased, when the scanning potential approached +1.0 V. As it went back to -0.2 V, it could be seen that there were two reduction peaks appeared at around +0.4 V and -0.1 V. These two peaks appeared due to the reduction of fully oxidized state (violet colored, pemigraniline base: PB) to half oxidized state (green colored, emeraldine salt: ES) at the first peak (+0.4 V) and the reduction of ES to fully reduced state (yellow colored, leucoemeraldine base: LB) at the second peak (-0.1 V). As the third cycle started and went to +1.0 V again, there was an oxidation peak appeared at around +0.25 V due to the oxidation of LB to ES and at +1.0 V, the ES oxidized to PB. As the oxidation of ES to PB occurred, the polymerization of aniline has occurred simultaneously, followed by an increase in current density of the reduction and oxidation peaks at the next cycle. As the CV scan was repeated, the polymerization potential shifted toward the lower potential, thus shifting the oxidation and reduction peaks to the more positive potential, this indicates that the polymerization process can now proceed at this lower potential. This is due to the increasing amount of PANI deposited on the LSGO surface with every cycle scanned. Subsequent growth of PANI occurred around the nuclei that were created at the early stage of polymerization. The reduction an oxidation peak of PANI from one to another structure also increased with increasing amount of PANI formed on LSGO [25].

The PBS/LSGO/PANI/LSGO/PBS ECD can be switched from the yellow color (fully reduced state of PANI) to the deep blue color (fully oxidized state of PANI) by applying potentials between 1.0 V and -0.6 V (Fig. 10). It has four different colors, yellow colored LB, green colored ES, blue colored EB (emeraldine base, half oxidized state) and finally, deep blue or violet colored PB. The most stable and conducting amongst the four oxidation states is green colored ES [39].

Fig. 10. Photos of the PBS/LSGO/PANI/LSGO/PBS ECD showing different colors at different voltages

For PLA/LSGO/PProDOT-Me_2/LSGO/PLA ECD experiments, the in situ method involves the production of electrochromic polymer inside a solid gel matrix of a constructed device. Fig. 4 shows a schematic showing how the in situ procedure works. First, a solution consisting of low molecular weight liquid monomer electrolyte and electrochromic monomer were placed between two LSGO-coated PLA substrates. Next, the acrylate functionalities were coupled using UV irradiation to produce a solid gel matrix. In the final step, a positive potential sufficient to polymerize the electroactive monomer was applied, generating the electrochromic polymer within the solid gel matrix nearest the LSGO working electrode [24]. Generally, switching a device from one state to the other is an electrochemical process dependent on several factors, such as the ionic conductivity of the gel electrolyte, ion diffusion in the polymer itself, and polymer film thickness and morphology [40]. An electrochromic polymer/gel electrolyte composite layer was formed during in situ polymerization. Entanglement with the cross-linked chains

may restrict the motion of polymer chains within this thin layer of gel electrolyte. Current versus time curve of the ECD is shown in Fig. 11. The bleached and colored states were obtained by biasing the EC layer at ± 1 V with respect to the counter electrode. The currents causing the coloration and bleaching of the ECD decay within 5 s. The PLA/LSGO/PProDOT-Me_2/LSGO/PLA devices exhibited good optical modulation, in which the color of the device switched from dark blue to a fully transparent state with the applied potential.

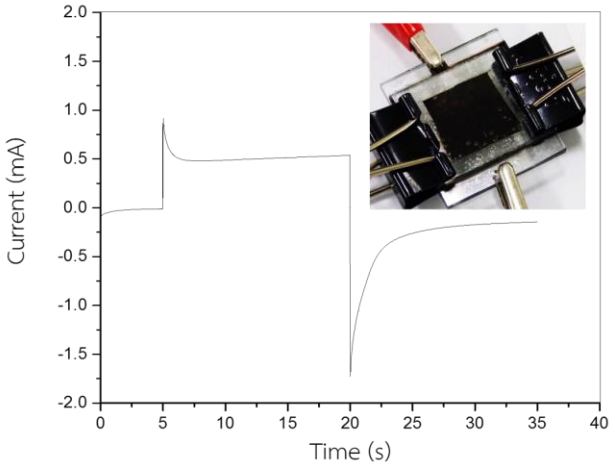

Fig. 11. Current versus time graph (the figure inset is a photograph of the colored state of the PLA/LSGO/PProDOT-Me_2/LSGO/PLA ECD

Based on the results, flexibility and electrochemical properties of the graphene derivative nanosheet could be tuned easily by adjusting constituent of mixture. Furthermore, the LSGO-coated biopolymer flexible films could be directly employed as electrode materials for ECD. This method could be applied to other materials as well.

4. Conclusions

The laser irradiation process resulted in the removal of oxygen species and the reestablishment of the sp^2 carbons. These caused a change in the conductivity of the sample from the insulating GO to highly conducting LSGO-10. The number of times a film was laser-treated resulted in a significant and controllable change in conductivity. In addition, the modified LSGO/biopolymer electrode was used as the supporting electrode of PProDOT-Me_2 or PANI ECD for the first time. Compared with ITO coated glass slide, LSGO coated PBS or PLA electrodes had higher resistance and lower transmittance. However, they exhibited higher flexibility and biodegradability. The TCE showed several advantages, such as simple preparation procedure, high sensitivity and flexibility, low detection limit and good reproducibility. The thin films of PProDOT-Me_2 and PANI were the promising anodic materials for ECD due to their good adhesion, transparency and EC. Overall, this new configuration presented an easy, expeditious and green way of preparing environment-friendly ECD.

Acknowledgements

This work is supported by Higher Education Research Promotion (HERP# 2558A11462008). The authors also wish to thank Department of Materials Science and Engineering, Faculty of Engineering and Industrial Technology, Silpakorn University and Center of Excellence on Petrochemical and Materials Technology, Chulalongkorn University for supporting and encouraging this investigation.

References

[1] S. K. Deb, Solar Energy Materials and Solar Cells **92**, 245 (2008).
[2] D. Evecan, O. Gurcuoglu, E. O. Zayim, Microelectronic Engineering **128**, 42 (2014).
[3] J. Wang, X. W. Sun, Z. Jiao, Materials **3**, 5029 (2010).
[4] R. H. Ma, Y. C. Chen, Sensors **12**, 359 (2012).
[5] C. X. Xu, K. J. Huang, Y. Fan, Z. W. Wu, J. Li, T. Gan, Materials Science and Engineering C **32**, 969 (2012).
[6] F. T. Thema, M. J. Moloto, E. D. Dikio, N. N. Nyangiwe, L. Kotsedi, M. Maaza, M. Khenfouch, Journal of Chemistry **2013**, Article ID 150536 (2013).
[7] R. Arvidsson, D. Kushnir, S. Molander, B. A. Sandén, Journal of Cleaner Production **132**, 289 (2016).
[8] A. Buasri, J. Patwiwattanasiri, N. Adisaisakunchai, A. Kemngen, V. Loryuenyong, Optoelectron. Adv. Mat. **9**, 507 (2015).
[9] K. Krishnamoorthy, G. S. Kim, S. J. Kim, Ultrasonics Sonochemistry **20**, 644 (2013).
[10] V. Strong, S. Dubin, M. F. El-Kady, A. Lech, Y. Wang, B. H. Weiller, R. B. Kaner, ACS Nano **6**, 1395 (2012).
[11] K. Griffiths, C. Dale, J. Hedley, M. D. Kowal, R. B. Kaner, N. Keegan, Nanoscale **6**, 13613 (2014).
[12] M. F. El-kady, V. Strong, S. Dubin, R. B. Kaner, Science **335**, 1326 (2012).
[13] Y. Chen, J. Xu, Y. Yang, Y. Zhao, W. Yang, X. He, S. Li, C. Jia, Journal of Materials Science: Materials in Electronics. **27**, 2564 (2016).
[14] D. S. Choi, S. H. Han, H. Kim, S. H. Kang, Y. Kim, C. M. Yang, T. Y. Kim, D. H. Yoon, W. S. Yang, Nanotechnology. **25**, 395702 (2014).
[15] A. Buasri, N. Chaiyut, V. Loryuenyong, N. Jaritkaun, T. Yavilas, N. Yoorengdech, Optoelectron. Adv. Mat. **7**, 938 (2013).
[16] A. Buasri, V. Loryuenyong, Optoelectron. Adv. Mat. **9**, 61 (2015).
[17] H. D. Huang, P. G. Ren, J. Z. Xu, L. Xu, G. J. Zhong, B. S. Hsiao, Z. M. Li, Journal of Membrane Science **464**, 110 (2014).

[18] D. M. Welsh, A. Kumar, E. W. Meijer, J. R. Reynolds, Advanced Materials **11**, 1379 (1999).
[19] J. Wu, X. Shen, L. Jiang, K. Wang, K. Chen, Applied Surface Science **256**, 2826 (2010).
[20] V. Loryuenyong, K. Totepvimarn, P. Eimburanapravat, W. Boonchompoo, A. Buasri, Advances in Materials Science and Engineering **2013**, Article ID 923403 (2013).
[21] H. Tian, Y. Shu, Y. L. Cui, W. T. Mi, Y. Yang, D. Xieab, T. L. Ren, Nanoscale **6**, 669 (2014).
[22] J. Song, X. Wang, C. T. Chang, Journal of Nanomaterials **2014**, Article ID 276143 (2014).
[23] A. Watanabe, G. Qin, J. Cai, Journal of Photopolymer Science and Technology **28**, 99 (2015).
[24] Y. Zhu, M. T. Otley, F. A. Alamer, A. Kumar, X. Zhang, D. M. D. Mamangun, M. Li, B. G. Arden, G. A. Sotzing, Organic Electronics **15**, 1378 (2014).
[25] M. F. Zainal, Y. Mohd, R. Ibrahim, 2013 IEEE Business Engineering and Industrial Applications Colloquium (BEIAC), Langkawi, Malaysia, 7-9 April 2013, p. 64.
[26] Y. Jin, M. Jia, M. Zhang, Q. Wen, Applied Surface Science **264**, 787 (2013).
[27] X. Su, G. Wang, W. Li, J. Bai, H. Wang, Advanced Powder Technology **24**, 317 (2013).
[28] M. Wojtoniszak, X. Chen, R. J. Kalenczuk, A. Wajda, J. Łapczuk, M. Kurzewski, M. Drozdzik, P. K. Chu, E. Borowiak-Palen, Colloids and Surfaces B: Biointerfaces **89**, 79 (2012).
[29] Y. Si, E. T. Samulski, Nano Letters **8**, 1679 (2008).
[30] Y. Shen, T. Jing, W. Ren, J. Zhang, Z. G. Jiang, Z. Z. Yu, A. Dasari, Composites Science and Technology **72**, 1430 (2012).
[31] B. Subramanya, D. Krishna Bhat, Journal of Power Sources **275**, 90 (2015).
[32] V. S. Channu, R. Bobba, R. Holze, Colloids and Surfaces A: Physicochemical and Engineering Aspects **436**, 245 (2013).
[33] S. Eigler, C. Dotzer, A. Hirsch, Carbon **50**, 3666 (2012).
[34] R. Ramachandran, M. Saranya, V. Velmurugan, B. P. C. Raghupathy, S. K. Jeong, A. N. Grace, Applied Energy **153**, 22 (2015).
[35] K. Wang, L. Li, X. Wu, International Journal of Electrochemical Science **8**, 6763 (2013).
[36] J. Guerrero-Contreras, F. Caballero-Briones, Materials Chemistry and Physics **153**, 209 (2015).
[37] A. Rani, S. Nam, K. A. Oh, M. Park, Carbon Letters **11**, 90 (2010).
[38] C. X. Xu, K. J. Huang, Y. Fan, Z. W. Wu, J. Li, Journal of Molecular Liquids **165**, 32 (2012).
[39] R. J. Mortimer, A. L. Dyer, J. R. Reynolds, Displays **27**, 2 (2006).
[40] A. A. Argun, P. H. Aubert, B. C. Thompson, I. Schwendeman, C. L. Gaupp, J. Hwang, N. J. Pinto, D. B. Tanner, A. G. MacDiarmid, J. R. Reynolds, Chemistry of Materials **16**, 4401 (2004).

*Corresponding author: achanai130@gmail.com; vorrada@gmail.com